nature geoscience

ARTICLES

PUBLISHED ONLINE: 18 JANUARY 2009 | DOI: 10.1038/NGEO416

Climate sensitivity to the carbon cycle modulated by past and future changes in ocean chemistry

Philip Goodwin[1,2]*, Richard G. Williams[1]*, Andy Ridgwell[3] and Michael J. Follows[4]

The carbon cycle has a central role in climate change. For example, during glacial–interglacial cycles, atmospheric carbon dioxide has altered radiative forcing and amplified temperature changes. However, it is unclear how sensitive the climate system has been to changes in carbon cycling in previous geological periods, or how this sensitivity may evolve in the future, following massive anthropogenic emissions. Here we develop an analytical relationship that links the variation of radiative forcing from changes in carbon dioxide concentrations with changes in air–sea carbon cycling on a millennial timescale. We find that this relationship is affected by the ocean storage of carbon and its chemical partitioning in sea water. Our analysis reveals that the radiative forcing of climate is more sensitive to carbon perturbations now than it has been over much of the preceding 400 million years. This high sensitivity is likely to persist into the future as the oceans become more acidic and the bulk of the fossil-fuels inventory is transferred to the ocean and atmosphere.

The carbon cycle is widely accepted as providing a pivotal role in the Earth's climate system[1], as illustrated by glacial–interglacial cycles over the past 400,000 years[2,3] (Fig. 1). Rising atmospheric CO_2 increases radiative forcing by enhancing the absorption and emission of infrared radiation[4]. In understanding this connection between radiative forcing and carbon cycling, the atmosphere cannot be viewed in isolation, as atmospheric CO_2 is rapidly exchanged with the ocean and terrestrial carbon systems. The ocean is the largest of these carbon reserves, 60 times larger than the atmospheric budget and 20 times larger than the terrestrial ecosystem and soils[1]. The air–sea exchange of CO_2 is altered by ocean chemistry with ocean uptake hindered by ocean acidification[1,5,6]. Here, we present a new analytical framework to elucidate the relationship between radiative forcing and CO_2 input to the atmosphere and oceans over millennial timescales, which is affected by the ocean storage of carbon and its chemical partitioning in sea water. This framework complements existing climate–carbon model studies applied to the geological past[7–11], addressing present anthropogenic change[12,13] and predicting millennia into the future[14–17].

To develop this framework, we start with the well-established link between radiative forcing and rising atmospheric CO_2 concentrations, as represented by[1,4]

$$\Delta F = \alpha \ln\left(\frac{C_{CO_2}}{C_o}\right) \quad (1)$$

where ΔF represents the rise in radiative forcing (in $W\,m^{-2}$) as atmospheric CO_2 increases in concentration from a reference value C_o to a new value C_{CO_2} (in $mol\,kg^{-1}$) and α measures the radiative characteristics of the atmosphere and is assumed here to be invariant. Adding progressively more CO_2 to the atmosphere eventually has a diminishing effect on radiative forcing as the wavelengths at which CO_2 can absorb become saturated, reflected by the logarithmic relationship in equation (1).

Changes in atmospheric CO_2 cannot be viewed in isolation, as there is a relatively rapid exchange with the ocean's reservoir of dissolved inorganic carbon (DIC). To link to the radiative forcing in equation (1), a change in atmosphere–ocean carbon inventory, ΔI (PgC), is defined here as the sum of the increase in the carbon stored in the atmosphere as CO_2 and in the ocean as saturated DIC (see the Methods section). ΔI can increase either by (1) external inputs of carbon added to the air–sea system or (2) internal ocean changes altering atmospheric CO_2 and saturated DIC. The external inputs to the air–sea system are from emissions or a reduction in the carbon stored in the terrestrial ecosystem. The internal changes reflect how atmospheric CO_2 and saturated DIC increases as ocean waters become more saturated or as biological export of carbon to the deep ocean weakens (see the Methods section).

For the first time, we now relate the radiative forcing ΔF ($W\,m^{-2}$) to changes in this atmosphere–ocean carbon inventory, ΔI (PgC),

$$\Delta F = \left(\frac{\alpha}{I_B}\right) \Delta I \quad (2)$$

The response of the radiative forcing to a change in the atmosphere–ocean carbon inventory ΔI is modulated by the ratio α/I_B, where α represents the variation of radiative forcing with atmospheric CO_2 and I_B reflects the dependence of ocean carbon storage on carbonate chemistry (discussed fully later). This relationship equation (2) applies only on millennial timescales as the atmosphere, ocean and terrestrial carbon systems approach a steady state[14,16,17].

To understand this long-term response, consider the transient adjustment of atmospheric CO_2 after perturbation in a simple carbon-cycle model[9] either by anthropogenic carbon emission (Fig. 2a) or a reduction in ocean biology (Fig. 2b). In both experiments, atmospheric CO_2 rises rapidly over the first few hundred years and then gradually approaches air–sea equilibrium after about 1,000 years. The inventory of atmospheric CO_2 and saturated DIC in the ocean increases ($\Delta I > 0$) through either the external input of carbon (Fig. 2a) or the internal changes

[1]Department of Earth and Ocean Sciences, University of Liverpool, Liverpool, L69 3GP, UK, [2]School of Environmental Sciences, University of East Anglia, Norwich, NR4 7TJ, UK, [3]School of Geographical Sciences, University of Bristol, Bristol, BS8 1SS, UK, [4]Department of Earth, Atmosphere and Planetary Sciences, Massachusetts Institute of Technology, Cambridge, Massachusetts 02139, USA. *e-mail: p.goodwin@uea.ac.uk; ric@liv.ac.uk.

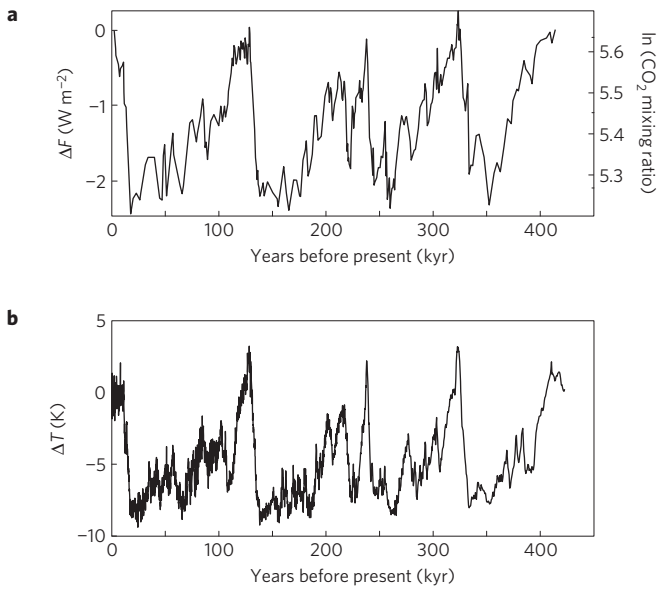

Figure 1 | Inferred changes in atmospheric CO_2, radiative forcing and temperature from ice-core records. a, Change in the logarithm of the mixing ratio of atmospheric CO_2 (ppm) over the past 400,000 years from the Vostok ice core[2] (right axis) together with the implied change in radiative forcing, ΔF (W m^{-2}, left axis) compared with the pre-industrial assuming $\alpha = 5.4$ W m^{-2} equation (1). **b**, Reconstructed local temperature change, ΔT, from the deuterium record[2]. The changes in radiative forcing associated with the variations in atmospheric CO_2 reach 1–2 W m^{-2}, and act to amplify the temperature changes, providing a positive feedback.

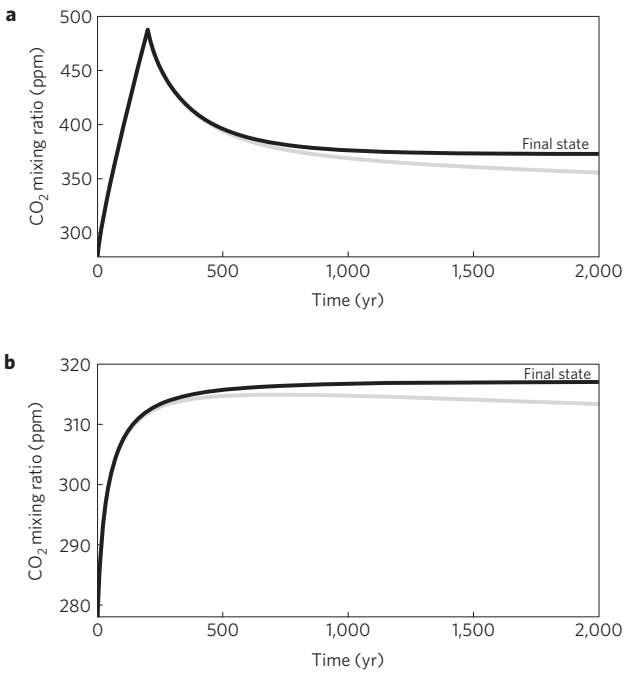

Figure 2 | Transient response of atmospheric CO_2 to idealized perturbations. a,**b**, The evolution of the atmospheric CO_2 mixing ratio (ppm) over 2,000 years from an external input of carbon from emissions (**a**) and from an internal change where surface DIC increases through a reduction in biological cycling (**b**). These perturbations are applied to the GENIE-1 Earth system model[9] integrated with (grey) or without (black) interactive sediments. In **a**, an emission of 1,000 PgC is spread evenly over 200 years into a pre-industrial spin-up, whereas in **b**, the reduction in ocean biological transfer is achieved by halving the maximum biological utilization of dissolved phosphate. When there are no interactive sediments, the atmospheric CO_2 approaches a steady state on a millennial timescale. This final state is determined by the increase in atmosphere–ocean carbon inventory ΔI given in **a** by how much carbon is released in emissions and in **b** by the reduction in biological export of carbon to the deep ocean. If this experiment is repeated with interactive sediments, there is a slight reduction in atmospheric CO_2 over a thousand years. Note that in **a**, atmospheric CO_2 initially exceeds the final equilibrium until sufficient time has passed for the ocean to sequester the extra CO_2 added to the system.

from weakening of the biological transfer of carbon to the deep ocean (Fig. 2b). The final concentration of atmospheric CO_2 is exponentially related to this atmosphere–ocean carbon inventory, ΔI (PgC), such that $C_{CO_2} = C_o \exp(\Delta I / I_B)$ (refs 18,19) and equation (2) hold. This air–sea equilibrium state is eventually modified by sediment and weathering interactions, which become increasingly important on longer timescales[7,16,17] (Fig. 2, grey line).

The buffered carbon inventory

The relationship between radiative forcing and changes in atmosphere–ocean carbon inventory in equation (2) depends on that inventory and the effect of ocean chemistry. To understand the role of ocean chemistry, consider the effect of more CO_2 being added to the ocean–atmosphere system. In the ocean, dissolved inorganic carbon, DIC $= [CO_2^*] + [HCO_3^-] + [CO_3^{2-}]$, is the sum of aqueous CO_2 and carbonic acid given by CO_2^*, bicarbonate, HCO_3^-, and carbonate, CO_3^{2-}, ions, with an equilibrium ratio of approximately 1:100:10 for pre-industrial conditions[7]. As CO_2 is added, the oceans become more acidic, the relative concentration of CO_2^* increases and CO_3^{2-} decreases[5,6]. This increase in CO_2^* acts to inhibit further ocean uptake of CO_2.

The buffering effect between atmospheric and ocean reservoirs of carbon is represented by the buffered carbon inventory, I_B, defined by the initial steady-state amount of CO_2 in the atmosphere, I_A (PgC), added to the amount of DIC in the ocean, I_O (PgC), divided by the Revelle buffer factor of sea water, B (dimensionless):

$$I_B = I_A + (I_O / B) \tag{3}$$

where B is defined as the fractional change in CO_2^* per unit fractional change in DIC as CO_2 is added to sea water[5],

$$B = \frac{\delta[CO_2^*]/[CO_2^*]}{\delta \mathrm{DIC}/\mathrm{DIC}}$$

B is typically 12 for the present surface ocean, but can rise to 18 with increased ocean acidity[6,20]. The buffered carbon inventory is dominated by the ocean contribution and the effect of ocean chemistry. For example, under pre-industrial conditions, the atmospheric carbon inventory I_A is only 600 PgC, dwarfed by the ocean inventory I_O of about 35,000 PgC (ref. 1). However, the buffered carbon inventory I_B is typically an order of magnitude smaller, ~3,500 PgC (ref. 18).

The effect of the different carbonate species on the buffered carbon inventory I_B is more clearly revealed by combining equation (3) with an approximation for the buffer factor, $B \approx \mathrm{DIC}/([CO_2^*] + [CO_3^{2-}])$ (see Supplementary Information), such that

$$I_B \approx \frac{M[CO_2^*]}{k_0} + V([CO_2^*] + [CO_3^{2-}]) \tag{4}$$

where M is the molar mass of the atmosphere, V is the volume of the ocean and k_0 relates $[CO_2^*]$ to the atmospheric CO_2 concentration at equilibrium, $C_{CO_2} = [CO_2^*]/k_0$. Hence, the buffered carbon inventory depends on the relative magnitudes of CO_2^* and carbonate, CO_3^{2-}, ions. For the present day, the carbonate

contribution dominates over that from CO_2^*, but the relative size of each contribution alters with the acidity of the oceans.

The sensitivity of radiative forcing to the carbon cycle

Ice-core records of glacial–interglacial cycles provide considerable insight into the coupling of the carbon cycle and climate (Fig. 1). Here our aim is to assess how representative our understanding of these relatively recent events is when considering past geological periods or the future after massive anthropogenic CO_2 release. To answer this question, we define the sensitivity of the radiative forcing to changes in the air–sea carbon inventory by rearranging equation (2), as

$$\frac{\Delta F}{\Delta I} = \frac{\alpha}{I_B} \quad (5)$$

which relates the radiative forcing for a specified change in air–sea carbon inventory, $\Delta F/\Delta I$, to the radiative characteristics of the atmosphere, α, divided by the buffered carbon inventory, I_B.

To test our theoretical framework, we compare our predictions for the sensitivity in radiative forcing to carbon changes equation (5) against independent numerical integrations of an Earth system model (GENIE-1; see the Methods section; ref. 21). A carbon perturbation is applied to the numerical model and then integrated for 1,000 years. This process is repeated many times covering a wide range of different initial states with different carbon inventories. Most of the transient adjustment of atmospheric CO_2 occurs over the first 200 years in the model (Fig. 2). After 1,000 years, the atmospheric CO_2 has approached an equilibrium state and the radiative forcing in the numerical model is determined from equation (1) assuming a modern-day α of 5.4 W m^{-2} (ref. 4). To understand the sensitivity of the radiative forcing, consider two types of perturbation.

First, consider the effect of carbon emissions, relevant to the future climate state unless substantive carbon capture is developed. For a carbon emission of 1,000 PgC, the GENIE-1 model integrations predict an increase in radiative forcing ranging from 1.7 to 0.7 W m^{-2} (Fig. 3a, dots). The higher radiative forcing occurs when I_B is small and the lower forcing when I_B is large, in accord with the analytical relationship between radiative forcing and the buffered carbon inventory equation (5) (Fig. 3a, line). With respect to the modern-day era, I_B is typically between 3,100 and 3,500 PgC (refs 18,19), leading to a relatively large radiative forcing of 1.5–1.7 W m^{-2} for the carbon emission of 1,000 PgC.

Second, consider changes in the marine biological drawdown of CO_2 into the ocean interior, which have been invoked to explain a significant fraction of the glacial–interglacial cycle in CO_2 (ref. 22) (Fig. 1). Doubling the efficiency with which surface nutrients are consumed and exported as sinking particles enhances the efficiency of the ocean's biological carbon pump. This reduces atmospheric CO_2 and weakens radiative forcing by −0.8 to −0.2 W m^{-2} (Fig. 3b, light dots and crosses). A weakening of the biological carbon pump increases atmospheric CO_2 and radiative heating by a similar magnitude (Fig. 3b). The magnitude of the response in radiative forcing varies inversely with the buffered carbon inventory (Fig. 3b, light dashed line).

This numerical experiment demonstrates that the idealized relationship equation (5) has quantitative predictive skill and illustrates how radiative forcing is modulated by the buffered carbon inventory. The theory is equally valid for inventory changes in the terrestrial ecosystem or ocean carbon disequilibrium, but the relation becomes more complicated if there are changes in calcium carbonate cycling (as the charge balance of the ocean is altered)[19].

Future effect of carbon emissions

To understand the effect of today's anthropogenic emissions on the sensitivity of the radiative forcing in equation (5), again consider

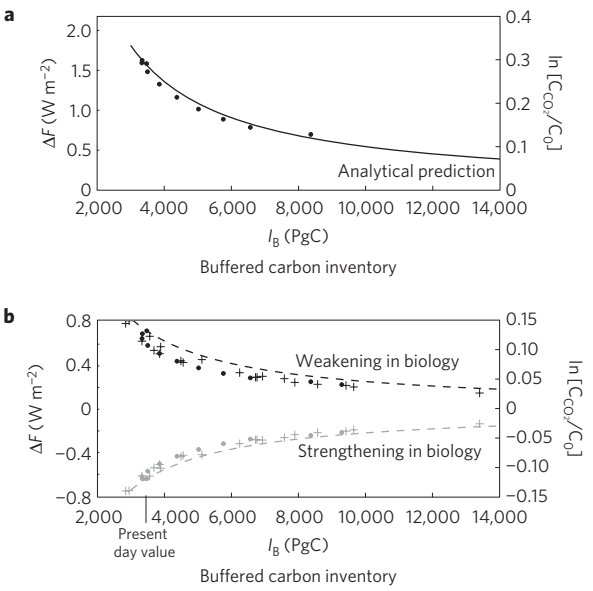

Figure 3 | Sensitivity of radiative forcing to the buffered carbon inventory following idealized perturbations. a,**b**, Change in radiative forcing ΔF (W m^{-2}) on a millennial timescale versus the buffered carbon inventory, I_B (PgC), for carbon-cycle perturbations involving carbon emissions (**a**) and changes in ocean biology (**b**). Analytical predictions (lines) are compared to separate numerical model integrations of the Earth system GENIE-1 model. The change in radiative forcing (left axis) is determined from atmospheric CO_2 (shown as $\ln(C_{CO_2}/C_0)$ in right axis) assuming a modern-day α. In **a**, an emission of $\Delta I = 1{,}000$ PgC is applied, whereas in **b** the biological changes include either a doubling (grey) or halving (black) of the maximum rate of biological phosphate utilization. These perturbations are applied to future states (dots) where only the total carbon inventory is altered and a series of palaeo-reconstructions (crosses) where both the total carbon and alkalinity are varied. The change in radiative forcing found in the numerical model integrations closely follows the theoretical prediction of an inverse relationship to I_B (lines).

the effects of ocean chemistry. For additions of CO_2 up to 4,000 PgC, the increase in CO_2^* is offset by a decrease in CO_3^{2-}, which leads to the buffered carbon inventory I_B remaining surprisingly constant in equation (4) (Fig. 4). In this case, radiative forcing remains highly sensitive to perturbation of the carbon cycle. This regime is relevant to the present day, where conventional carbon reserves are being used, as these reserves are estimated to reach up to 5,000 PgC (ref. 23).

However, for additions of CO_2 greater than 4,000 PgC, the increase in CO_2^* dominates over the decrease in CO_3^{2-} and thus, I_B eventually increases in equation (4). In this regime, the sensitivity of radiative forcing to a further perturbation of the carbon cycle is eventually reduced even though CO_2 is increasingly transferred into the atmosphere (Fig. 4). This regime with an increase in carbon inventory of >4,000 PgC is relevant to our likely far future state after conventional fossil fuels are exhausted and in the absence of substantive carbon capture.

Past modulation of radiative-forcing sensitivity

Now consider how the sensitivity of radiative forcing to changes in carbon cycling might vary over geologic time. This question is addressed by applying relations (4) and (5) together with reconstructions of the buffered carbon inventory I_B (determined from the GENIE-1 model; see the Methods section[21]).

Palaeo-reconstructions suggest atmospheric CO_2 concentrations have been much higher over much of the past 400 Myr compared with the pre-industrial[24] (Fig. 5a, dots). This increase in

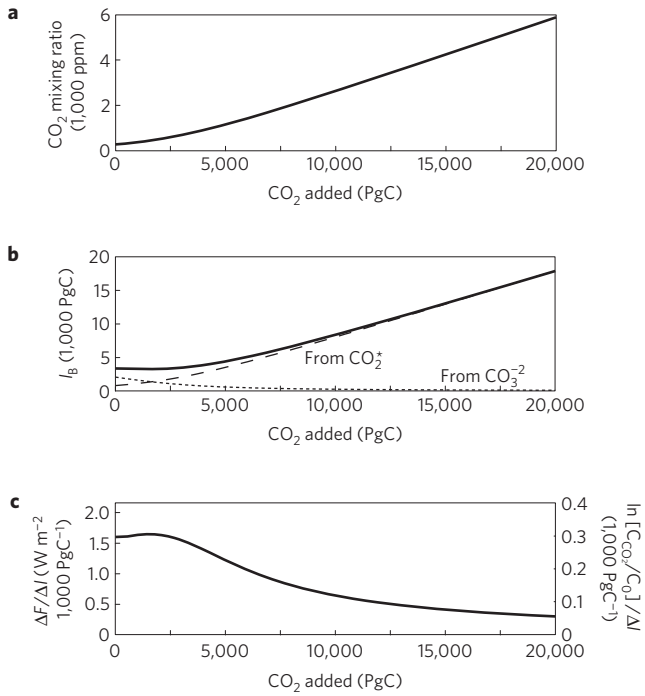

Figure 4 | Future possible changes in atmospheric CO_2, carbon inventory and sensitivity of radiative forcing. a, Rise in atmospheric CO_2 (ppm) as CO_2 (PgC) is added to a simplified air–sea box model. **b**, Buffered carbon inventory I_B (black, 1,000 PgC) versus CO_2 addition together with the contributions to I_B from $[CO_3^{2-}]$ (short dashed) and $[CO_2^*]$ (long dashed). **c**, Sensitivity of radiative forcing to carbon inventory changes, $\Delta F/\Delta I$ (W m^{-2}/1,000 Pg C^{-1}) versus CO_2 addition (left axis), assuming a modern-day α, together with $\ln(C_{CO_2}/C_0)/\Delta I$ (1,000 PgC^{-1}; right axis). In **b**, for the first 4,000 PgC added, I_B remains hardly changed (black line), because the increase in contribution from CO_2^* is offset by a decrease in contribution from CO_3^{2-}. For further increases in CO_2 greater than 4,000 PgC, the sensitivity of radiative forcing eventually diminishes as I_B increases.

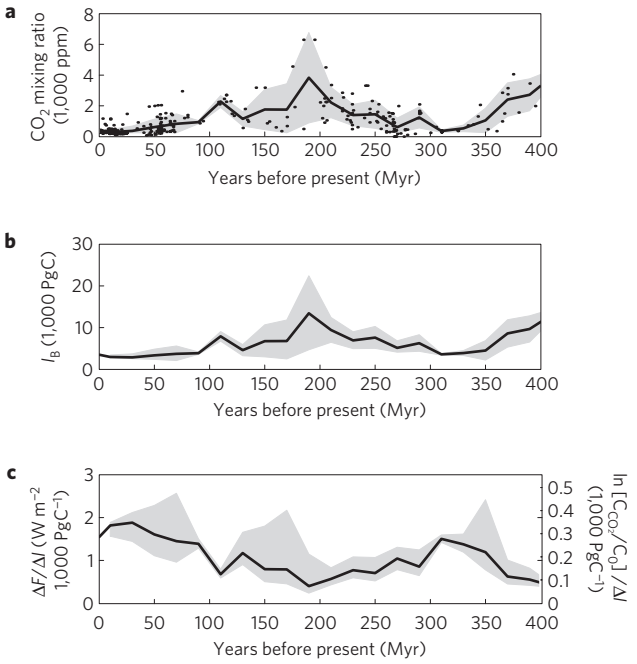

Figure 5 | Past inferred changes in atmospheric CO_2, carbon inventory and sensitivity of radiative forcing. a, Past inferences over the past 400 Myr for the mixing ratio of atmospheric CO_2 (1,000 ppm) determined from proxy data (black dots)[24], averaged[8] to give mean (black solid line), high and low values (grey shaded area). **b**, Reconstruction of the buffered carbon inventory I_B (black, 1,000 PgC) evaluated using the GENIE-1 model (see the Methods section). **c**, Analytical predictions for the sensitivity of the radiative forcing to air–sea carbon inventory changes, $\Delta F/\Delta I$ (W m^{-2} 1,000 PgC^{-1}) (left axis) assuming a modern-day α, together with $\ln(C_{CO_2}/C_0)/\Delta I$ (1,000 PgC^{-1}; right axis). Grey shading represents the uncertainty resulting from the estimates of atmospheric CO_2.

atmospheric CO_2 concentration leads to CO_2^* concentrations likewise being much larger, whereas $CaCO_3$ weathering and sedimentation constraints have prevented ocean $CaCO_3$ saturation falling far below pre-industrial levels[8–10]. The inferred changes in ocean chemistry caused I_B, equation (4), to be much larger for much of the past 400 Myr compared with the pre-industrial era (Fig. 5b). Thus, the radiative forcing induced from a carbon perturbation equation (5) would have been relatively small over the earlier part of this past record (Fig. 5c). At its peak 200 Myr ago, I_B reached ~3–4 times pre-industrial levels, reducing the sensitivity of radiative forcing to carbon inventory changes by up to 75% compared with the present-day value (Fig. 5c). This reduction in radiative forcing reflects a substantial weakening in the past ability of the carbon cycle to influence climate by altering atmospheric CO_2. Conversely, over the past 200 Myr, there has been a long-term decline in atmospheric CO_2 and I_B leading to an increased sensitivity of radiative forcing.

This palaeo-reconstruction of I_B has implications for the interpretation of past global warming events and assessing their relevance for future climate sensitivity[25,26]. For example, 55 Myr ago, there was a global warming and carbon release event, lasting from 1 to 10 kyr, referred to as the Palaeocene–Eocene Thermal Maximum[27,28]. As the Palaeocene–Eocene Thermal Maximum event had a similar I_B to the pre-industrial (Fig. 5b), this event provides a useful analogy for the present-day scenario of warming from anthropogenic emissions.

Implications for climate–carbon cycle feedbacks

The effect of the carbon cycle on radiative forcing is influenced both by the storage of carbon within the ocean and the buffering by ocean chemistry. When the buffered carbon inventory I_B is small, there is a relatively large radiative forcing of climate for any given perturbation to the carbon cycle and, thus, there is a potential for strong positive feedback between climate and carbon cycling. When the buffered carbon inventory I_B is large, there is a relatively small radiative forcing for a given perturbation to the carbon cycle and, thus, potential for only weak positive feedback.

The radiative forcing exerted by atmospheric CO_2 changes during glacial–interglacial cycles probably reflects the present-day sensitivity of radiative forcing to carbon-cycle changes. For the present day, a recent comparison of 11 coupled climate–carbon cycle models reveals a positive feedback between carbon and climate in all cases[13]: the inclusion of the carbon cycle leading to enhancement of global warming of between 0.1 °C and 1.5 °C in projections over the next 100 years. However, this high sensitivity need not have always applied further back in the geologic past owing to changes in the buffered carbon inventory I_B.

Our study suggests that the influence of changes to the carbon cycle on climate is stronger now than over much of the past 400 Myr and will remain strong in the near future with fossil-fuel CO_2 release and ocean acidification. For the modern era, we suggest that for every 1,000 PgC emitted to the atmosphere, there will be

an added radiative forcing of 1.5 W m^{-2} lasting for millennia. In a similar way, terrestrial carbon and ocean ecosystem feedbacks can potentially modify this radiative forcing by up to about 30% (refs 1,13). Consequently, it is an inopportune time to perturb the carbon system. The relationships developed here provide an elegant way to reveal the climate sensitivity to the carbon system and should be viewed as the first part of a model hierarchy to understand how the coupled carbon–climate system operates[29].

Methods

Definition of carbon inventories. The total amount of carbon in the Earth's atmosphere and ocean, ΣC, is given by the sum of their inventories, I_A and I_O,

$$\Sigma C = I_A + I_O = MC_{CO_2} + V\overline{DIC} \quad (6)$$

which can be written in terms of atmospheric concentration of carbon dioxide, C_{CO_2} (mol kg^{-1}), M is the molar mass of the atmosphere, V is the volume of the ocean, and the average dissolved inorganic carbon concentration, $\overline{DIC}$ (mol m^{-3}). The ocean DIC can be separated into different components reflecting the effect of different processes[30,31]

$$DIC = C_{sat} + C_{dis} + C_{bio} + C_{CaCO_3} \quad (7)$$

where C_{sat} defines the saturation concentration of DIC if the surface water is in equilibrium with the atmosphere, C_{dis} represents the amount of disequilibrium between surface water and the atmosphere, C_{bio} represents the increase in DIC from the remineralization of biological soft tissue and C_{CaCO_3} represents the increase in DIC from dissolution of calcium carbonate, hard tissue.

If small perturbations to the inventory equation (6) are now considered using equation (7), with changes in calcium carbonate cycling ignored for simplicity, then we can write[19,31]

$$M\Delta C_{CO_2} + V\left(\Delta\overline{C_{sat}} + \Delta\overline{C_{dis}} + \Delta\overline{C_{bio}}\right) = \Delta\Sigma C \quad (8)$$

where an overbar represents a whole ocean average. By assuming that an increase in the total atmosphere–ocean carbon inventory ($\Delta\Sigma C$) may be due to anthropogenic carbon emissions (ΔI_{em}) or a contraction of the terrestrial carbon reservoir (ΔI_{ter}), then equation (8) can be rearranged as

$$M\Delta C_{CO_2} + V\Delta\overline{C_{sat}} = \Delta I_{em} - \Delta I_{ter} - V\left(\Delta\overline{C_{dis}} + \Delta\overline{C_{bio}}\right) \equiv \Delta I \quad (9)$$

ΔI measures the change in the atmosphere–ocean carbon inventory from an increase in atmospheric CO_2 and the increase in saturated DIC, given by the left-hand side of equation (9). ΔI can be viewed as representing the response of the system on a millennial timescale to the perturbations imparted on the system, given by the right-hand side of equation (9). ΔI is increased by external inputs of carbon to the air–sea system from emissions (ΔI_{em}) and contraction of the terrestrial reservoir (ΔI_{ter}). Likewise, ΔI increases from internal changes (with atmospheric CO_2 and saturated ocean DIC becoming larger) with a weakening in air–sea disequilibrium ($-V\Delta\overline{C_{dis}}$) or from a weakening in the biological transfer of carbon into the deep ocean ($-V\Delta\overline{C_{bio}}$).

This increase in atmosphere–ocean carbon inventory, ΔI, leads to an exponential rise in atmospheric CO_2 with a generic solution to equation (9) given by $C_{CO_2} = C_o \exp(\Delta I / I_B)$. This solution is valid as long as I_B is unchanged as the system is perturbed, $\Delta I_B \ll I_B$ (ref. 18).

Adding CO_2 to the pre-industrial system. We analyse how carbon emissions change atmospheric CO_2 and I_B at air–sea equilibrium using either a simplified air–sea box model[32] or the GENIE-1 Earth system model[21], which consists of a three-dimensional ocean circulation, a two-dimensional energy balance for the atmosphere and thermodynamic sea ice.

The simplified box model[6] is integrated to air–sea equilibrium with the mixing ratio of atmospheric CO_2 forced at 5 ppm intervals up to a maximum of 5,240 ppm At each of the separate steady states reached, the carbon emission and buffered carbon inventory, I_B (ref. 18) are determined.

The GENIE-1 Earth system model[21] was configured in a 'closed system' with no weathering gains or burial losses, and initialized with an atmospheric CO_2 of 278 ppm. Different carbon emissions were added to the atmosphere over one year from 0 to 10,000 PgC in 1,000 PgC steps. For each case, the model was integrated for 5,000 years until air–sea equilibrium is reached and I_B was determined. An 'open system' version of GENIE-1 (ref. 9) including weathering and sediment interactions was also used for Fig. 2.

Analysing the buffered carbon inventory, I_B, over the past 400 Myr. We estimate the climate sensitivity to CO_2 release over the past 400 Myr in the following manner. First, a box model of global carbon cycling was used to reconstruct the marine carbon cycle and concentrations of alkalinity and total DIC in the ocean at 20 Myr intervals over the past 400 Myr (ref. 8). The calculated alkalinity and DIC values assume an equilibrium with atmospheric CO_2 concentrations following a proxy data set[24], as well as influences due to past variations in weathering, oceanic calcium ion concentrations and area available for shallow-water carbonate deposition. In addition, no significant pelagic carbon production or burial is assumed before 200 Myr.

Second, the GENIE-1 Earth system model[21] was initialized from the proxy-derived CO_2 concentrations and predicted alkalinity and DIC values from ref. 8. GENIE-1 was run assuming a modern climatology and continental configuration for 5,000 years in a 'closed system' configuration to re-equilibrate ocean chemistry. The difference in the mean ocean DIC in GENIE-1 and the initialization from the box model[8] was less than 15 μmol kg^{-1}, revealing that both models had broadly consistent steady-state, global solutions. The buffered carbon inventory I_B in GENIE-1 was then determined[18] from the reconstruction of past ocean chemistry.

Inducing ocean biology changes in the GENIE-1 model. The effects of ocean biological changes were assessed by including enhanced or weakened biological cycling where the maximum conversion rate of phosphate into organic material was either doubled or halved. These biological perturbations were then separately applied to spin-ups generated at intervals over the past 400 Myr and future post-emission states of the GENIE-1 model[21]. Each time the model was integrated for 1,000 years without sediment interactions to obtain the equilibrium response for Fig. 3; in addition, a version of GENIE-1 (ref. 9) including weathering and sediment interactions was used for Fig. 2.

Received 25 July 2008; accepted 18 December 2008; published online 18 January 2009

References

1. IPCC 2007. *Climate Change 2007: The Physical Science Basis. Contribution of Working Group I to the Fourth Assessment Report of the Intergovernmental Panel on Climate Change* (Cambridge Univ. Press, 2007).
2. Petit, J. R. *et al.* Climate and atmospheric history of the past 420,000 years from the Vostok ice core, Antarctica. *Nature* **399**, 429–436 (1999).
3. Siegenthaler, U. *et al.* Stable carbon cycle-climate relationship during the late Pleistocene. *Science* **310**, 1313–1317 (2005).
4. Myhre, G., Highwood, E. J., Shine, K. P. & Stordal, F. New estimates of radiative forcing due to well mixed greenhouse gases. *Geophys. Res. Lett.* **25**, 2715–2718 (1998).
5. Bolin, B. & Eriksson, E. in *The Atmosphere and the Sea in Motion: Scientific Contributions to the Rossby Memorial Volume* (ed. Bolin, B.) 130–142 (Rockefeller Inst. Press, 1959).
6. The Royal Society. *Ocean Acidification Due to Increasing Atmospheric Carbon Dioxide*, Policy document 12/05, ISBN 0 85403 617 2 (The Royal Society, 2005); available at <www.royalsoc.ac.uk>.
7. Ridgwell, A. & Zeebe, R. E. The role of the global carbonate cycle in the regulation and evolution of the Earth system. *Earth Planet. Sci. Lett.* **234**, 299–315 (2005).
8. Ridgwell, A. A Mid Mesozoic revolution in the regulation of ocean chemistry. *Mar. Geol.* **217**, 339–357 (2005).
9. Ridgwell, A. Interpreting transient carbonate compensation depth changes by marine sediment core modeling. *Paleoceanography* **22**, PA4102 (2007).
10. Berner, R. A. A model for atmospheric CO_2 over Phanerozoic time. *Am. J. Sci.* **291**, 339–376 (1991).
11. Berner, R. A. & Kothavala, Z. GEOCARB III: A revised model of atmospheric CO_2 over Phanerozoic time. *Am. J. Sci.* **301**, 182–204 (2001).
12. Joos, F., Plattner, G-K, Stocker, T. F., Marchal, O. & Schmittner, A. Global warming and marine carbon cycle feedbacks on future atmospheric CO_2. *Science* **284**, 464–467 (1999).
13. Friedlingstein, P. *et al.* Climate carbon cycle feedback analysis: Results from the C4MIP model intercomparison. *J. Clim.* **19**, 3337–3353 (2006).
14. Lenton, T. M. *et al.* Millennial timescale carbon cycle and climate change in an efficient Earth system model. *Clim. Dyn.* **26**, 687–711 (2006).
15. Lenton, T. M. Land and ocean carbon cycle feedback effects on global warming in a simple Earth system model. *Tellus* **52B**, 1159–1188 (2000).
16. Archer, D. The fate of fossil fuel in geologic time. *J. Geophys. Res.* **110**, C09S05 (2005).
17. Archer, D., Kheshgi, H. & Maier-Reimer, E. Multiple timescales for neutralization of fossil fuel CO_2. *Geophys. Res. Lett.* **24**, 405–408 (1997).
18. Goodwin, P., Williams, R. G., Follows, M. J. & Dutkiewicz, S. Ocean-atmosphere partitioning of anthropogenic carbon dioxide on centennial timescales. *Glob. Biogeochem. Cycles* **21**, GB1014 (2007).
19. Goodwin, P., Follows, M. J. & Williams, R. G. Analytical relationships between atmospheric carbon dioxide, carbon emissions, and ocean processes. *Glob. Biogeochem. Cycles* **22**, GB3030 (2008).
20. Sabine, C. L. *et al.* The oceanic sink for anthropogenic CO_2. *Science* **305**, 367–371 (2004).

21. Ridgwell, A. *et al.* Marine geochemical data assimilation in an efficient Earth System Model of global biogeochemical cycling. *Biogeosciences* **4**, 87–104 (2007).
22. Sigman, D. M. & Boyle, E. A. Glacial/interglacial variations in atmospheric carbon dioxide. *Nature* **407**, 859–869 (2000).
23. Rogner, H. H. An assessment of world hydrocarbon resources. *Annu. Rev. Energy Environ.* **22**, 217–262 (1997).
24. Royer, D. L., Berner, R. A., Montanez, I. P., Tabor, N. J. & Beerling, D. J. CO_2 as a primary driver of Phanerozoic climate. *GSA Today* **14**, 4–10 (2004).
25. Pagani, M., Caldeira, K., Archer, D. & Zachos, J. C. An ancient carbon mystery. *Science* **314**, 1556–1557 (2006).
26. Panchuk, K., Ridgwell, A. & Kump, L. R. Sedimentary response to Paleocene-Eocene Thermal Maximum carbon release: A model-data comparison. *Geology* **36**, 315–318 (2008).
27. Kennett, J. P. & Stott, L. D. Abrupt deepsea warming palaeoceanographic changes and benthic extinctions at the end of the Paleocene. *Nature* **353**, 225–229 (1991).
28. Röhl, U., Bralower, T. J., Norris, R. D. & Wefer, G. New chronology for the late Paleocene thermal maximum and its environmental implications. *Geology* **28**, 927–930 (2000).
29. Held, I. The gap between simulation and understanding in climate models. *Bull. Am. Meteorol. Soc.* 1609–1614 (2005).
30. Brewer, P. G. Direct observation of the oceanic CO_2 increase. *Geophys. Res. Lett.* **5**, 997–1000 (1978).
31. Ito, T. & Follows, M. J. Preformed phosphate soft tissue pump and atmospheric CO_2. *J. Mar. Res.* **63**, 813–839 (2005).
32. Sarmiento, J. L. & Toggweiler, J. R. A new model for the role of the oceans in determining atmospheric P_{CO_2}. *Nature* **308**, 621–624 (1984).

Acknowledgements

This research was supported by NERC grants NE/F002408/1 and NE/F001657/1.

Author contributions

P.G., R.G.W. and M.J.F. contributed theory to the study and A.R. conducted the supporting numerical modelling with GENIE-1. P.G. and R.G.W. led the writing of this study, and contributed equally, together with inputs from A.R. and M.J.F.

Additional information

Supplementary Information accompanies this paper on www.nature.com/naturegeoscience. Reprints and permissions information is available online at http://npg.nature.com/reprintsandpermissions. Correspondence and requests for materials should be addressed to P.G. or R.G.W.

Supplementary material

Estimating I_B by deriving an approximation for the Revelle buffer factor

The Revelle buffer factor is formally defined as the fractional change in $[CO_2^*]$ divided by the fractional change in DIC concentration at constant temperature, salinity and carbonate alkalinity,

$$B = \frac{\delta[CO_2^*]/[CO_2^*]}{\delta \mathrm{DIC}/\mathrm{DIC}}. \quad \text{(S1)}$$

Consider the definitions of DIC and carbonate alkalinity, A_C,

$$\mathrm{DIC} = [CO_2^*] + [HCO_3^-] + [CO_3^{2-}], \quad \text{(S2)}$$

$$A_C = [HCO_3^-] + 2[CO_3^{2-}], \quad \text{(S3)}$$

where the DIC species partition with a pH dependence according to the first and second dissociation constants, K_1 and K_2,

$$K_1 = \frac{[H^+][HCO_3^-]}{[CO_2^*]}, \quad \text{(S4)}$$

$$K_2 = \frac{[H^+][CO_3^{2-}]}{[HCO_3^-]}. \quad \text{(S5)}$$

We wish to gain an expression for $\frac{\delta[CO_2^*]}{[CO_2^*]}$ from (S1). From (S4) and (S5), CO_2^* can be expressed

$$[CO_2^*] = \frac{K_2}{K_1}\frac{[HCO_3^-]^2}{[CO_3^{2-}]}. \quad \text{(S6)}$$

Noting that K_1 and K_2 do not change at constant temperature and salinity, (S6) can be differentiated using the chain rule to find,

$$\frac{\delta[CO_2^*]}{[CO_2^*]} = 2\frac{\delta[HCO_3^-]}{[HCO_3^-]} - \frac{\delta[CO_3^{2-}]}{[CO_3^{2-}]}. \quad \text{(S7)}$$

Now, assuming constant carbonate alkalinity implies,

$$\delta A_C = 0 = \delta[HCO_3^-] + 2\delta[CO_3^{2-}] \quad \text{(S8)}$$

which substitutes into (S7) to give,

$$\frac{\delta[CO_2^*]}{[CO_2^*]} = -\frac{\delta[CO_3^{2-}]}{[CO_3^{2-}]}\left(1 + 4\frac{[CO_3^{2-}]}{[HCO_3^-]}\right). \quad \text{(S9)}$$

In modern conditions, $[HCO_3^-]>>[CO_3^{2-}]$, therefore $\frac{\delta[CO_2^*]}{[CO_2^*]}$ becomes simply,

$$\frac{\delta[CO_2^*]}{[CO_2^*]} = -\frac{\delta[CO_3^{2-}]}{[CO_3^{2-}]}. \qquad \text{(S10)}$$

We can find an approximation for B by again considering the constant alkalinity constraint,

$$\delta A_C = 0 = \delta\mathrm{DIC} - \delta[CO_2^*] + \delta[CO_3^{2-}], \qquad \text{(S11)}$$

and substituting for δDIC in (S11), and for $\delta\,[CO_2^*]$ in (S10) into the definition of the Revelle buffer factor, (S1), to reveal,

$$B = \frac{\delta[CO_2^*]/[CO_2^*]}{\delta\mathrm{DIC}/\mathrm{DIC}} \approx \frac{\mathrm{DIC}}{[CO_2^*]+[CO_3^{2-}]}, \qquad \text{(S12)}$$

which is valid for fixed A_C, and $[HCO_3^-]>>[CO_3^{2-}]$, approximately corresponding to the pH range ~4.5 to 8.5.

Substituting (S12) into the definition of the buffered carbon inventory, $I_B=I_A+(I_O/B)$, gives

$$I_B \approx I_A + V\left([CO_2^*]+[CO_3^{2-}]\right) \qquad \text{(S13)}$$

where V is the volume of the ocean. Combining with Henry's Law relating seawater CO_2^* and the concentration of carbon dioxide of an overlying atmosphere C_{CO2} at equilibrium,

$$k_0 C_{CO2} = [CO_2^*], \qquad \text{(S14)}$$

where k_0 is a function of temperature and salinity, then leads to an approximation for I_B in terms of CO_2^* and CO_3^{2-},

$$I_B \approx \frac{M[CO_2^*]}{k_0} + V\left([CO_2^*]+[CO_3^{2-}]\right), \qquad \text{(S15)}$$

where M is the molar mass of the atmosphere.